THE UNIVERSITY OF MICHIGAN

SCHOOL OF DENTISTRY

Final Report

CALIBRATION OF SIX-CHANNEL INTRAORAL OCCLUSAL FORCES TRANSMITTERS

Major M. Ash
Ian S. Scott

ORA Project 07975

under contract with:

DEPARTMENT OF HEALTH, EDUCATION, AND WELFARE
PUBLIC HEALTH SERVICE
NATIONAL INSTITUTES OF HEALTH
CONTRACT NO. PH 43-66-511
BETHESDA, MARYLAND

administered through:

OFFICE OF RESEARCH ADMINISTRATION ANN ARBOR

March 1967

TABLE OF CONTENTS

	Page
OBJECTIVES	v
A. ANALYSES OF PROBLEMS	1
Introduction	1
Theoretical Considerations	1
B. CALIBRATION INSTRUMENTATION SYSTEM	9
System Description	9
C. ANALYSIS OF OCCLUSAL FORCE SENSORS	12
D. COMPARISON BETWEEN THEORETICAL PREDICTIONS AND OBSERVED READINGS	23
Alternate Sensor Configurations	23
E. DATA ANALYSIS PROCEDURE	24
Data Analysis Procedure	24
Calibration data	24
Raw data	24
F. SUMMARY	30

OBJECTIVES

The objectives of the contract were to: (1) generate theoretical analyses of the problems involved in calibrating the measurement of occlusal forces in six-channel intraoral transmitters developed under NIH Grant DE 1962-01-03, and determine the "best" arrangement for the occlusal forces sensors; (2) develop a device for calibrating the six-channel occlusal forces transmitters; (3) determine the force sensor outputs generated by different loads, velocity and related linearity; (4) compare theroetical predictions of sensor output with observed output derived with use of the calibration device; and (5) present a preliminary data analysis procedure including a data output format.

A. ANALYSES OF PROBLEMS

INTRODUCTION

The problem posed consists of attempting to measure forces between occlusal surfaces in contact. The way in which this will be done is to embed strain-sensitive gauges within a tooth, and measure the response of the system to surface forces. Quantitative predictions of the magnitude and location of the surface forces are to be made from the strain-gauge signals generated by the contact stresses.

The first part of this report will discuss theoretical analyses of the stresses and strains expected to be produced at the sensors, together with the effects of relative sensor geometry upon the generated signals, which will point to the "best" arrangements for the problem.

THEORETICAL CONSIDERATIONS

Before discussing the stress analysis, mention should be made of the strict definition of stress and strain, and of the sign conventions and symbolism used.

Stress may be thought of as the "force intensity" at a point. It is defined as the force ÷ the cross-sectional area over which the force acts. Two sorts of stress can be identified: "direct stresses" (σ) which act normally to the surface being considered, and "shear stresses" (τ) which act across such surfaces.

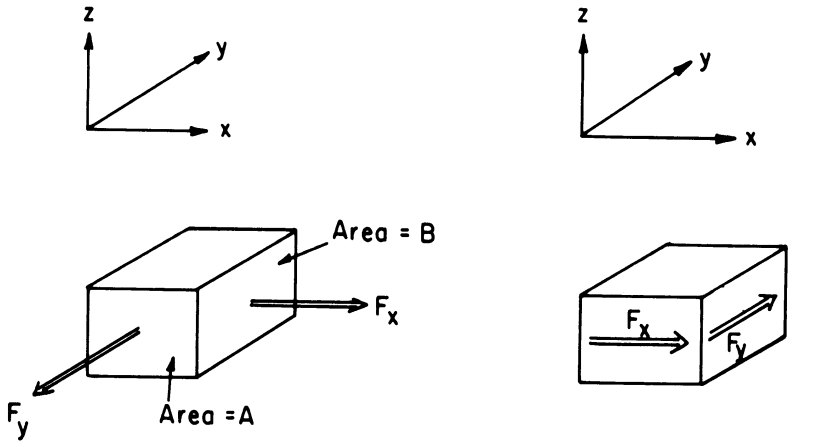

$$\sigma_x = \frac{F_x}{B} \qquad \sigma_y = \frac{F_y}{A} \qquad \tau_{xy} = \frac{F_x}{A} \qquad \tau_{yx} = \frac{F_y}{B}$$

Tensile forces are taken as positive. Compressive forces are taken as negative.

Strain is the relative deformation of a piece of material. "Normal" strains (produced by direct stresses) are conveniently defined in terms of the "change in length" of a reference length when acted upon by a normal force, e.g., if a length L of wire stretches by length ΔL, when acted upon by a normal force, the strain is

$$\epsilon = \Delta L/L$$

Shear strains (obviously caused by shear forces which try to change the shape of a body without changing its size) are conveniently defined by the change of attitude of a reference line, e.g., if a line is sheared over through an angle ϕ when acted upon by a shear force, the strain is

$$\gamma = \phi = \frac{\Delta h}{k}$$

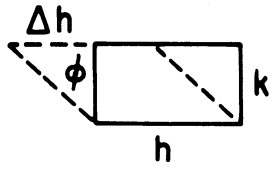

Stress and strain are related in elasticity by the so-called "elastic moduli." For direct stresses

$$\sigma = E \cdot \epsilon \text{ where E is Young's Modulus,}$$

and for shear stresses

$$\tau = G \cdot \gamma \text{ where G is the shear modulus.}$$

E and G are related themselves as follows

$$G = \frac{E}{2(1 + \nu)}$$

where ν is "Poisson's Ratio," and is defined formally by the ratio of $\left[\frac{\text{the lateral contraction strain}}{\text{the longitudinal extension strain}}\right]$, alluding to the fact that if something is stretched, it shrinks across a diameter.

Consequently, these relationships allow an understanding of the mechanical behavior of a solid when stressed, and predictions of strains and deformations may be made.

In connection with the present project, two problems in classical elasticity are relevant, (i) Boussinesq's problem, and (ii) Cerutti's problem.

Boussinesq considers a normal point load* active on the free surface of a half space.** The problem is simple conceptually (Figure 1) and although not so simple mathematically, is still the easiest to consider.

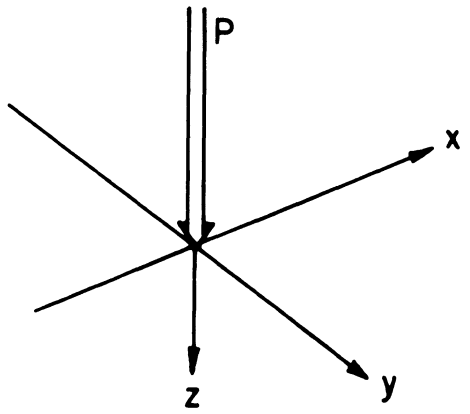

Figure 1

This situation is a first approximation to the condition of a normal force active on an occlusal surface. It is possible to derive expressions for the normal strains at any arbitrary point (which will be activating the sensors at those points) and we can then see how sensitive the system will be to various forms of loading. The normal load P acts at the origin of cartesian coordinates in the xy surface plane. The z direction is that of the line of applications of the force vector. At any point (x,y,z) the normal strains in the x,y, and z directions are as follows:

$$\epsilon_{xx} = \frac{P}{4\pi G}\left[\frac{z}{R^3} - \frac{3x^2z}{R^5} + \frac{(1-2\nu)}{R(R+z)}\left[\frac{x^2(2R+z)}{R^2(R+z)} - 1\right]\right]$$

$$\epsilon_{yy} = \frac{P}{4\pi G}\left[\frac{z}{R^3} - \frac{3y^2z}{R^5} + \frac{(1-2\nu)}{R(R+z)}\left[\frac{y^2(2R+z)}{R^2(R+z)} - 1\right]\right]$$

$$\epsilon_{zz} = \frac{P}{4\pi G} \cdot \frac{z}{R^3} \cdot \left[2\nu - \frac{3z^2}{R^2}\right]$$

G = shear modulus = $\frac{E}{2(1+\nu)}$ as before, and $R = \sqrt{x^2 + y^2 + z^2}$.

*A "point load" means a load acting over a vanishingly small area.
**A "half space" is analogous with a very large homogeneous block of material.

ϵ_{xx} and ϵ_{zz} may be plotted for various depths (z) below the surface, and in various planes (y) away from the point of application. Typical graphs for (z=1, y=0) are shown in Figures 2 and 3. These demonstrate that at a z level the strains may change sign, which will similarly alter the tensile-compressive response of the sensors.

The first approximation to the condition of a horizontal shearing force acting on an occlusal surface, is the classical problem of Cerutti, which considers a horizontal traction in the xy surface plane of the half space (xz, yz). Again, we may derive expressions for the normal strains at any arbitrary point which will be activating the sensors there.

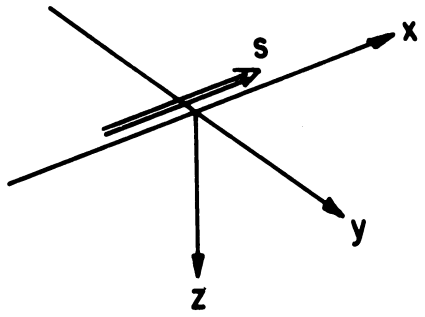

The horizontal load S acts at the origin of cartesian coordinates in the xy surface plane, in the direction of the x axis. At any point (x,y,z) the normal strains in the x, y, and z directions are as follows:

$$\epsilon_{xx} = \frac{S}{4\pi G}\left[\frac{x}{R^3} - \frac{3x^3}{R^5} - \frac{2(1-2\nu)x}{R(R+2)^2} + \frac{(1-2\nu)x^3\,(3R+z)}{R^3(R+z)^3} - \frac{(1-2\nu)x}{R(R+z)^2}\right]$$

$$\epsilon_{yy} = \frac{S}{4\pi G}\left[\frac{x}{R^3} - \frac{3xy^2}{R^5} - \frac{(1-2\nu)x}{R(R+z)^2} + \frac{(1-2\nu)xy^2\,(3R+z)}{R^3(R+z)^3}\right]$$

$$\epsilon_{zz} = \frac{S}{4\pi G}\left[2\nu \cdot \frac{x}{R^3} - \frac{3xz^2}{R^5}\right]$$

G = shear modulus = $\frac{E}{2(1+\nu)}$ as before, and $R = \sqrt{x^2 + y^2 + z^2}$.

One may plot these strains as with the strains due to a normal force, and one can demonstrate the change in sign of the sensor outputs.

For any arbitrary loading (into normal forces in the z direction and horizontal forces in the x and y directions), one may use the principle of linear elastic superposition to give the overall sensor effect. In practice, of course, the sensors are of a finite size and not simply a "point." Consequently, one should strictly integrate the actions at a point over the finite area of the sensor.

Again, the solutions given are for the "hypothetical" mathematical case of "point" loads. In reality, the load is distributed over a finite area,

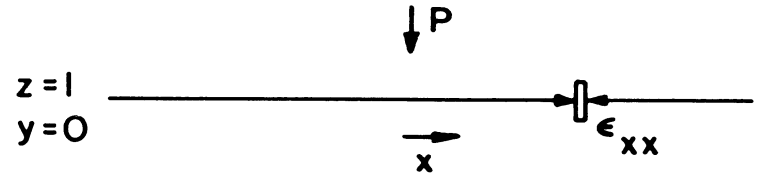

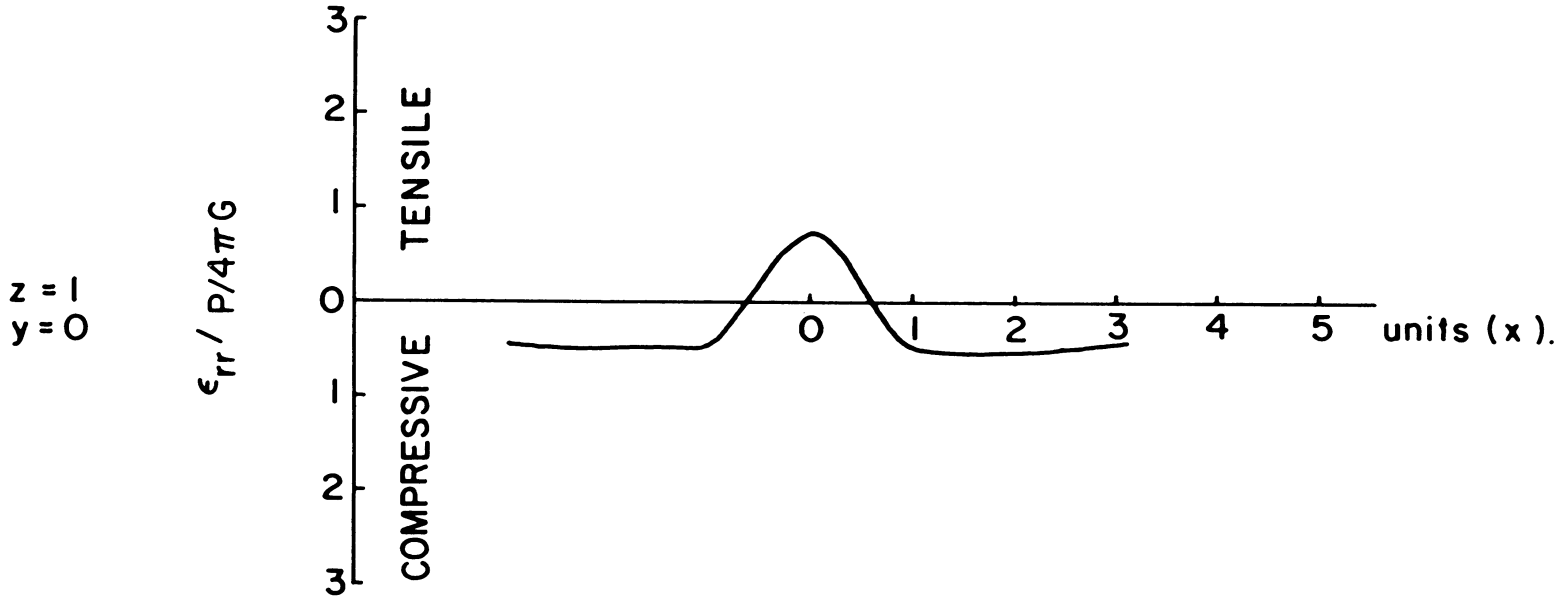

$$\epsilon_{xx} = \frac{P}{4\pi G}\left[\frac{2}{R^3} - \frac{3x^2 z}{R^5} + \frac{(1-2\nu)}{R(R+2)}\left[\frac{x^2(2R+2)}{R^2(R+2)} - 1\right].\right].$$

Figure 2

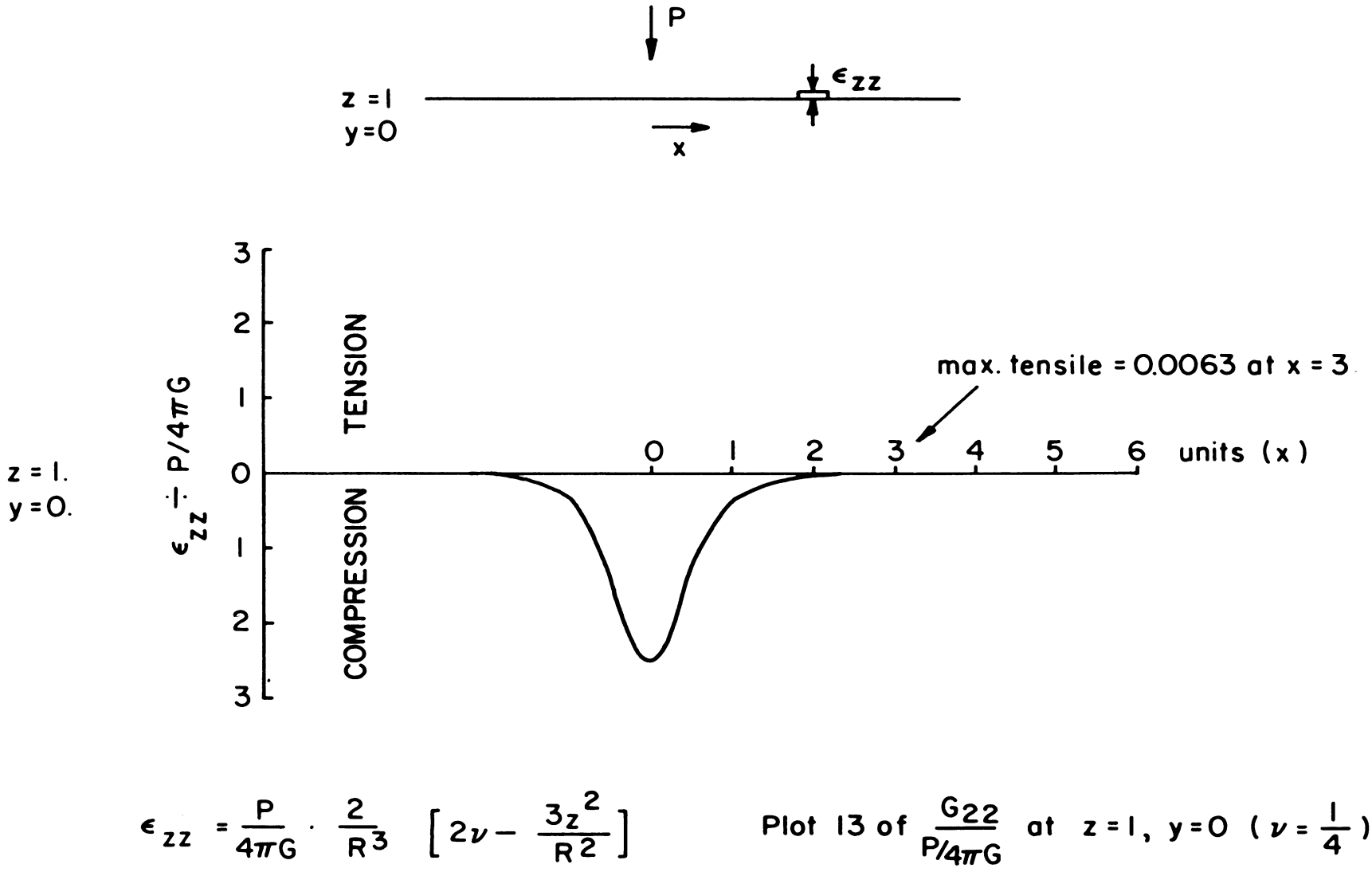

$$\epsilon_{zz} = \frac{P}{4\pi G} \cdot \frac{2}{R^3} \left[2\nu - \frac{3z^2}{R^2} \right]$$

Plot 13 of $\frac{G22}{P/4\pi G}$ at $z = 1$, $y = 0$ $\left(\nu = \frac{1}{4}\right)$

Figure 3

whence one should use the analysis of Hertz and its developments by Mindlin and Goodman. In principle, all that is necessary for a formal determination of the strain field is to write down the expressions for the state of strain due to the Boussinesq and Cerutti point forces, and to integrate over the plane z = 0 with appropriate weighting functions (depending on the distribution of stress over the finite contact region). Unfortunately, this direct approach leads to a series of intractable harmonic integrals. Solutions may be obtained but are quite complex and at the present time the subject of much intensive research. Because most of the differences between the "simple" solutions and reality concern the areas adjacent to the loaded area, and not at regions far away from it, it is felt that the Boussinesq and Cerutti solutions will be sufficient for the present problem. Moreover, it must be remembered that the practical sensor setup involves a combination of materials of differing elastic properties (occlusal material and channel material), the influence of which on the classical analysis is far from clear. Certainly, the real problem is intractable at the moment. The solution given does, however, give valuable pointers to what to expect.

The analysis does not take into account any time-dependent mechanical properties (i.e., creep behavior) and is essentially a quasi-static solution. It would seem essential to avoid the use of any material that would creep, since, apart from the virtual impossibility of incorporating any visco-elastic, history dependent, mechanical behavior into the analysis, the train sensor readings would just not make sense; a given reading could be caused by a "light load for a long time" or by a "heavy load in a short time," and repeated cyclic loadings will alter the visco-elastic response.

Consequently, if one can temporarily forget any practical manufacturing difficulties, "creepy" materials should not be used. If acrylic can be used, then it will be the simplest to apply, and presumably if it is much below the glass-transition temperature, it should not creep much under the loading being used. If necessary "completely rigid" occlusal surfaces should be made (surrounding the channel); with mouth temperatures normal encountered, gold would undoubtedly do, and any amalgam also providing it were below half the absolute temperature of the solidus point on its equilibrium diagram.

Typical values for the shear modulus of an acrylic polymer (e.g., PMM) would be 0.2×10^6 psi, and for gold would be 2×10^6 psi. For both, Poisson's ratio is roughly 1/3. In general terms, the acrylic will give a larger strain for the same loading arrangement.

It would appear that the idea of using a "gold cap" as the occlusal surface could work, but may lead to an irregularly sensitive system, in that the sensors are practically <u>at</u> the loading points. (It could, however, be held in reserve as a possibility.) The elasticity of the medium within the cap might produce interpretation problems.

Having explored the many ways of arranging the sensors within the tooth (paying particular emphasis on the possible need for asymmetry because of uniqueness problems), it is felt that for the particular information being requested, the six sensors should be arranged 4 vertical and 2 horizontal or 4 horizontal and 2 vertical depending on whether the side forces or downward forces are of greater interest.

In order to isolate the 2 components of force on each of 4 cusps, 8 sensors (1 vertical and 1 horizontal, under each cusp) would be required.

B. CALIBRATION INSTRUMENTATION SYSTEM

SYSTEM DESCRIPTION

The system is composed of five main subsystems

1. The precision XY table
2. SLO-SYN indexers
3. XY recorder
4. Force control
5. TM receiver/discriminators

1. The precision XY table was designed to move the occlusal force transmitter in an XY plane, in either a continuous or intermittent mode. A scanning plot may be obtained on the XY recorder of each sensor output for a given force applied. The XY table is fabricated to withstand any anticipated forces and will be able to be repositioned to the starting point after each series of scans to within $\pm$ 0.002.

2. The X and Y axis indexing motors operate independently of each other and the XY system is comprised of the basic elements shown in Figure 4. These include an adjustable frequency oscillator, control gates, decade counters, and a pulse-to-step translator logic circuit. Depending on the positioning movement desired the correct count is present on the decade counter controls. A command signal in the form of a switch closure causes the gate circuits to pass pulses from the oscillator to the decade counters and the translator logic circuit. The translator logic circuit converts the pulses into the correct switching sequence needed to advance the motor shaft in steps of 1.8° when the count (single scan) is complete. The control gate turns off the pulse gate and actuates the relay to: (1) reverse motor direction; (2) remove scanning force; (3) actuate the X axis step; and (4) return the Y axis to the start of the scan position. On completion of the return to start of scan position, the control gate turns on the scanning force and restarts the scanning cycle.

3. The XY recorder is coupled to the XY table by substituting the usually manually operated zero control potentiometers with potentiometers coupled to the X and Y axes of the XY table. This system provides a complete dynamic range of the XY recorder without interfering with the input signals.

4. The force control subsystem has been designed to provide a continuously variable force over a range of 0-100 lb and has excellent damping characteristics. The subsystem is comprised of an air hydraulic piston spring loaded in a retracted position along with pressure regulating values and electrically

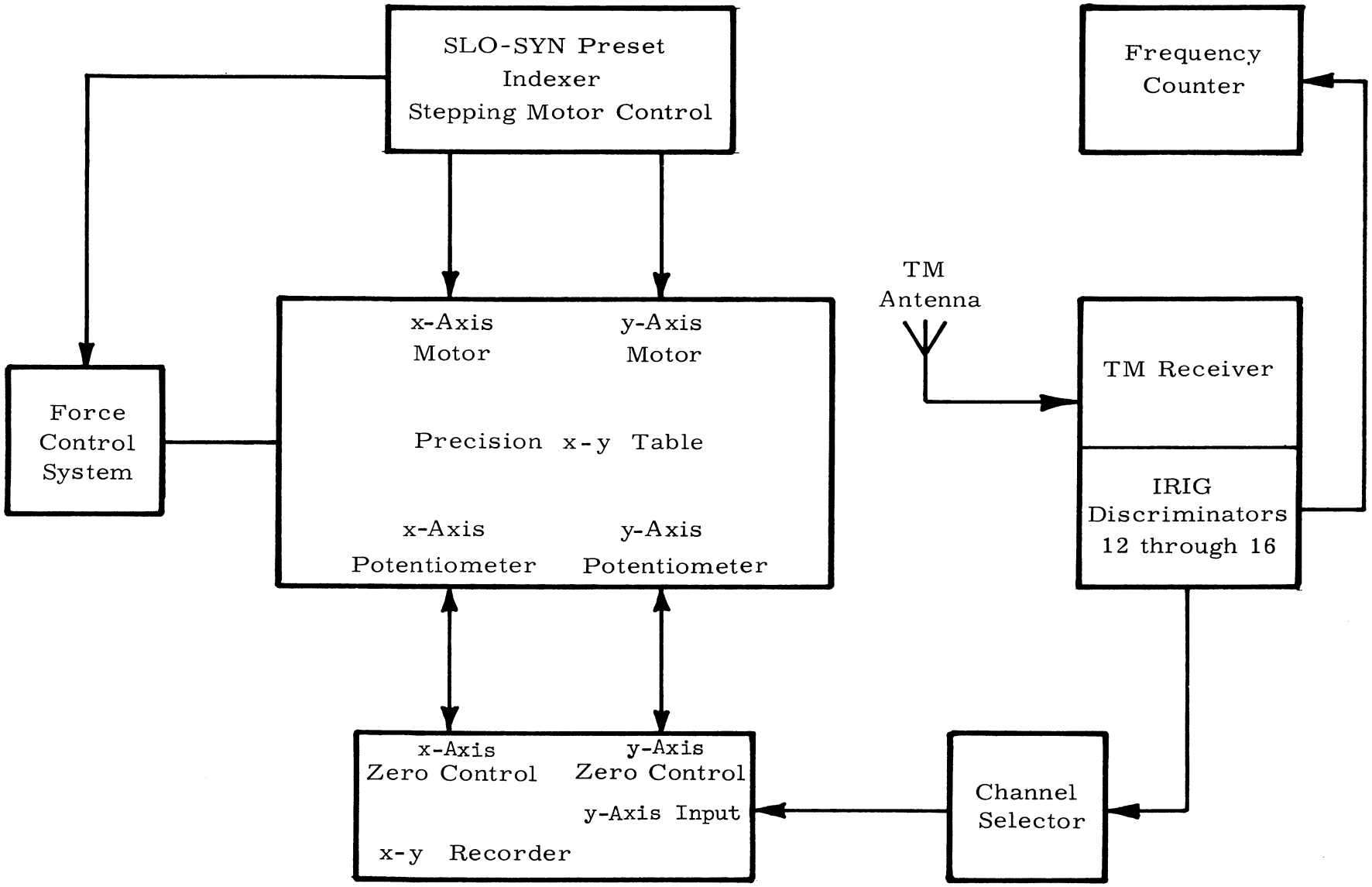

Figure 4. Occlusal force calibration system.

operated on-off switches. Very precise force values can be obtained through double regulation.

5. The telemetry system consists of a telemetry receiver, six discriminators, channel selector, and frequency counter. The initial operation consisted of selecting one of the six channels to be displayed on the XY plotter and checking the channel IRIG frequency and then running a complete scan of the transmitter occlusal surface. This operation was repeated for all six channels in both the continuous and intermittent modes until an accurate display had been obtained for all six sensor outputs.

C. ANALYSIS OF OCCLUSAL FORCE SENSORS

The first consideration was to compare the mathematical analysis of the tensile-compressive response of the sensors to actual output using the calibration device.

Therefore, six sensors were mounted in a standard "U" channel sensor mount (see Figure 5) and covered with acrylic to form a flat surface over the entire sensor area. Channels 2 and 4 of the six-channel sensor pack (Figure 5) was scanned by the XY force scanner and force variations recorded on the X axis of the XY recorder. The responses are shown in Figures 6, 8, and 10. After evaluation of a flat surface, a molar occlusal surface was added and the sensor pack was scanned again. These outputs are shown in Figures 7, 9, and 11. The last calibration step was to scan a six-channel transmitter, the output of one sensor is shown in Figures 12 and 13.

The response of the sensors to various traverse loading speeds was tested. The results are shown in Figure 14.

The magnification of the occlusal surface is 20X as seen on the graphs in the original data plot. However, due to the printing process size limitations the graph data has been made smaller to fit into the report.

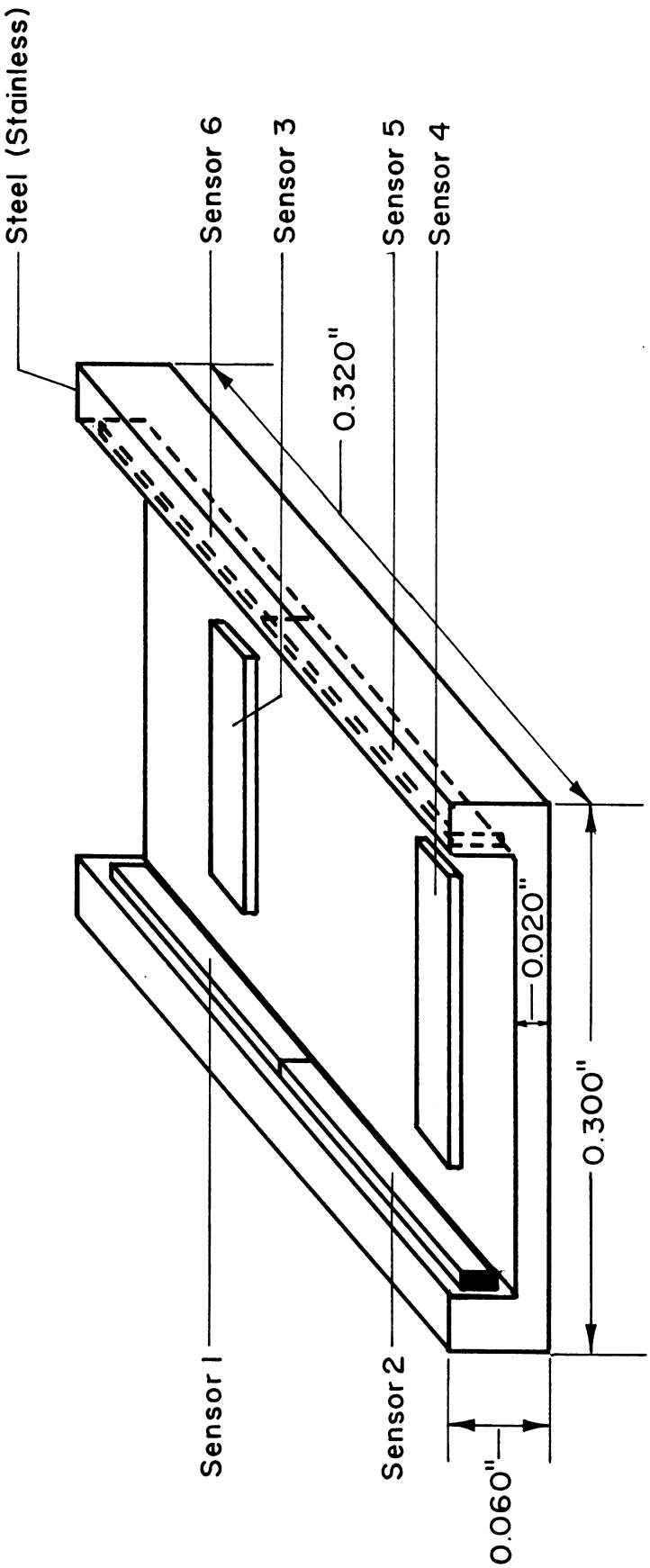

Figure 5. Force sensor configuration.

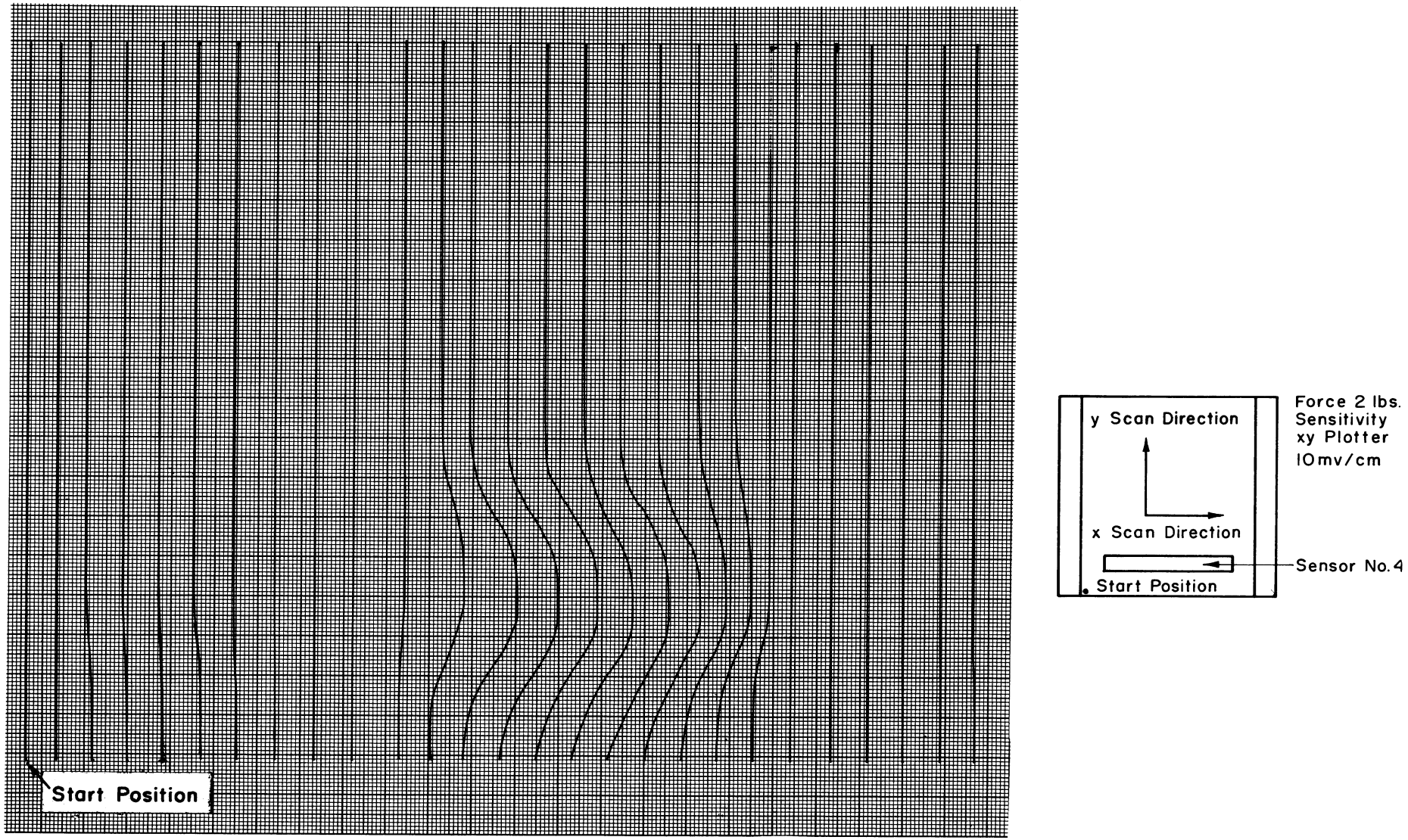

Figure 6. Flat occlusal surface.

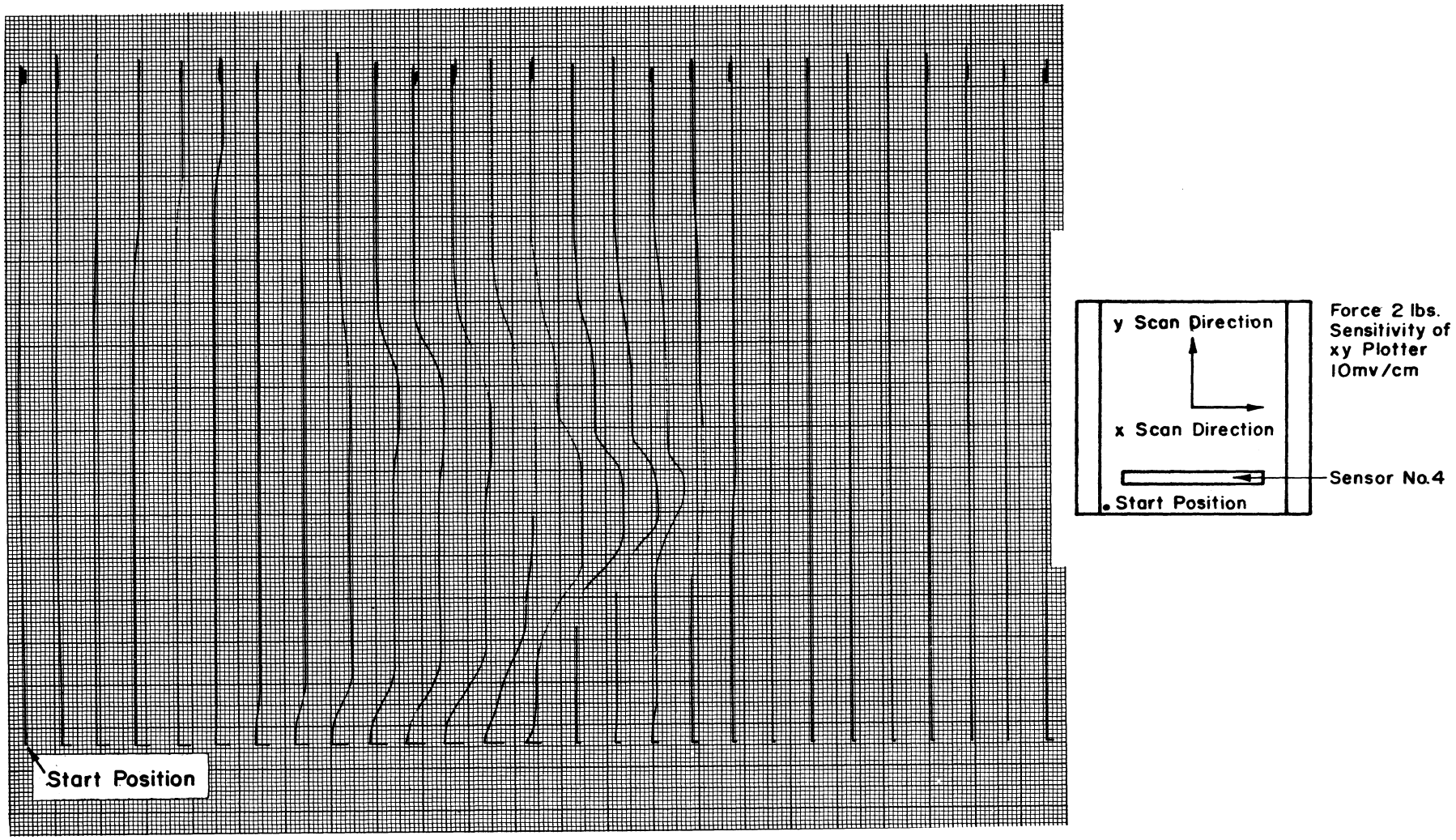

Figure 7. Normal occlusal surface.

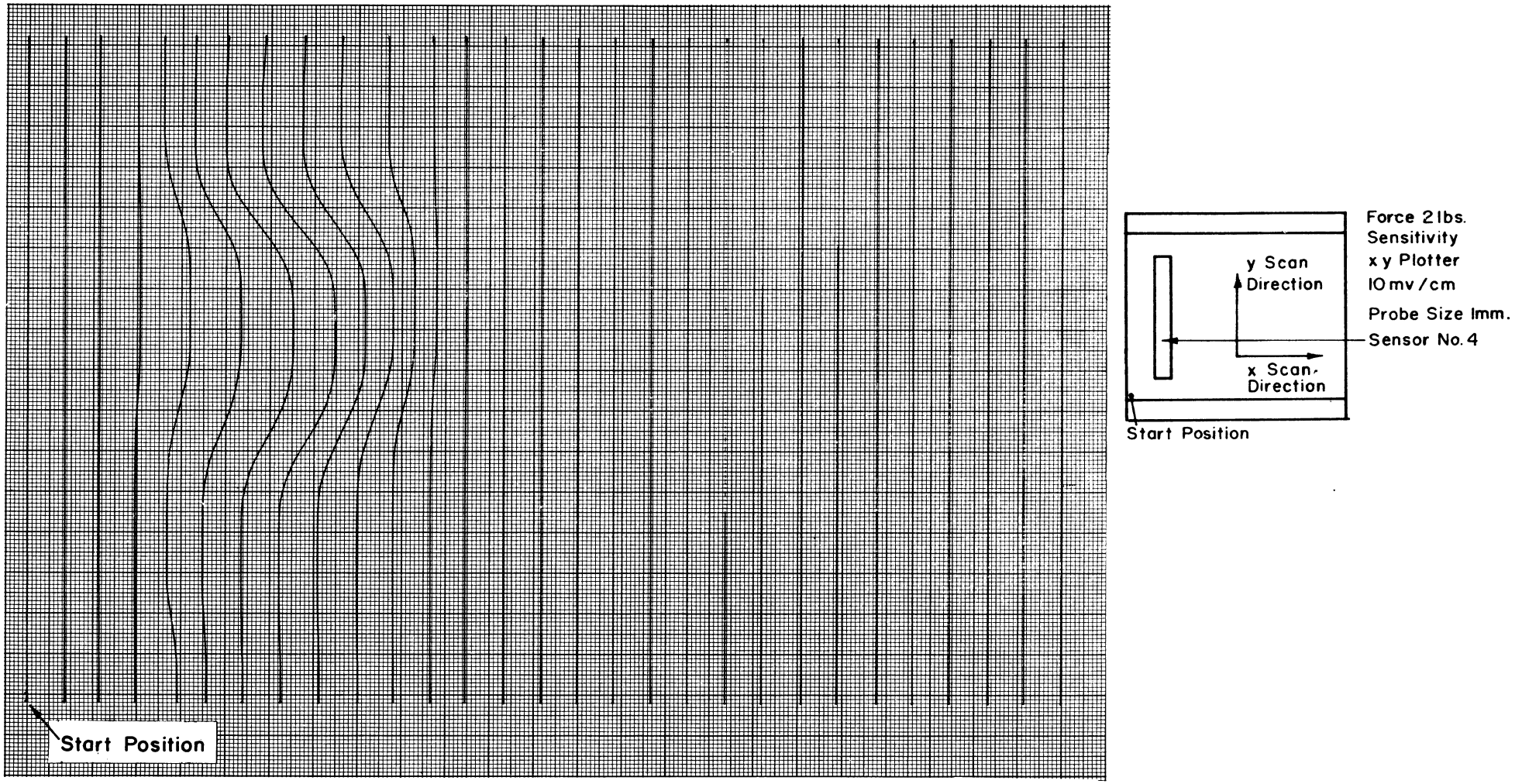

Figure 8. Flat occlusal surface.

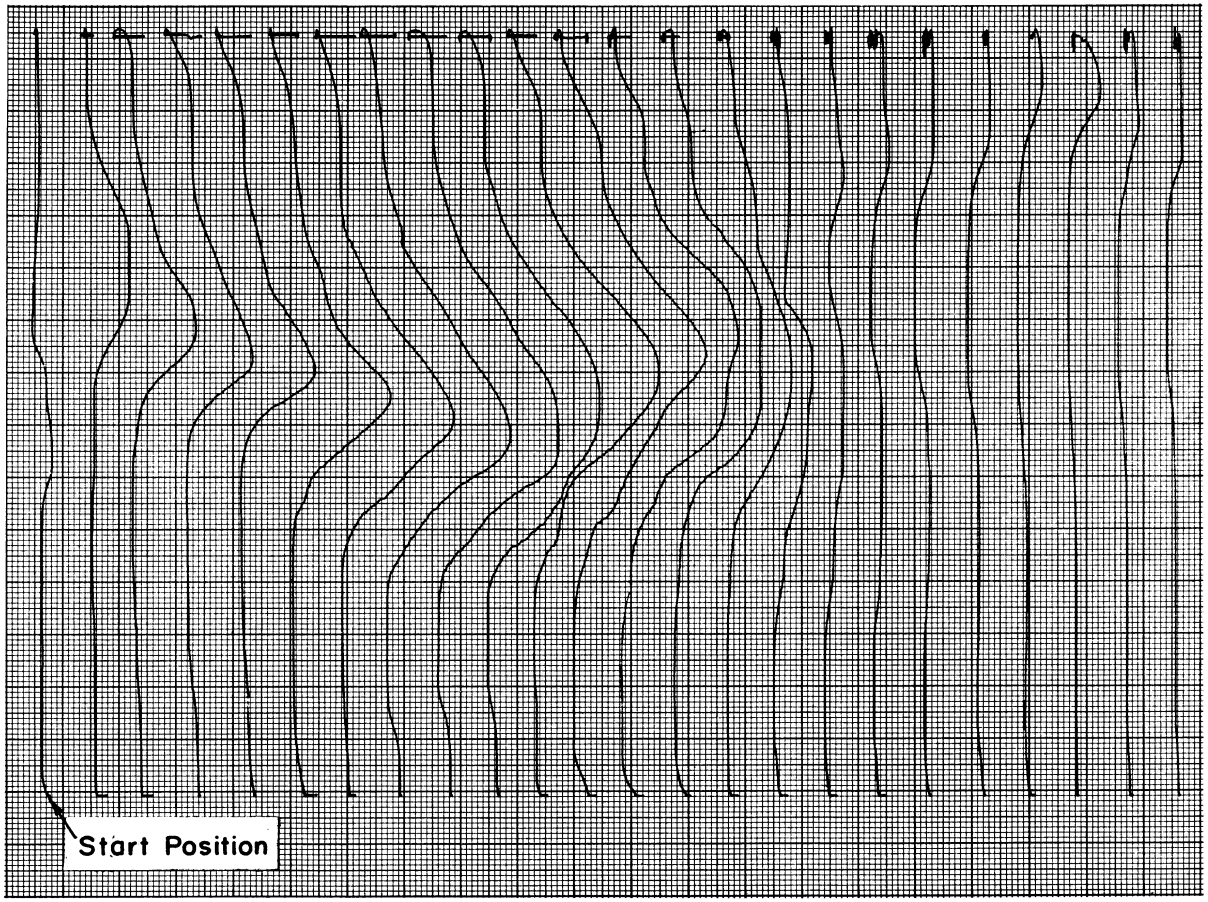

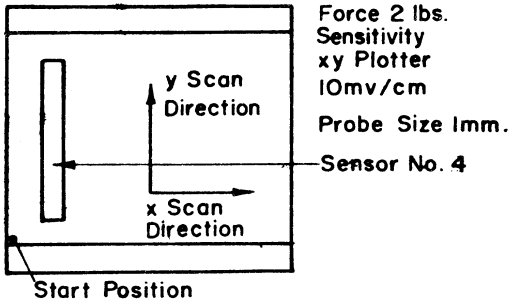

Figure 9. Normal occlusal surface.

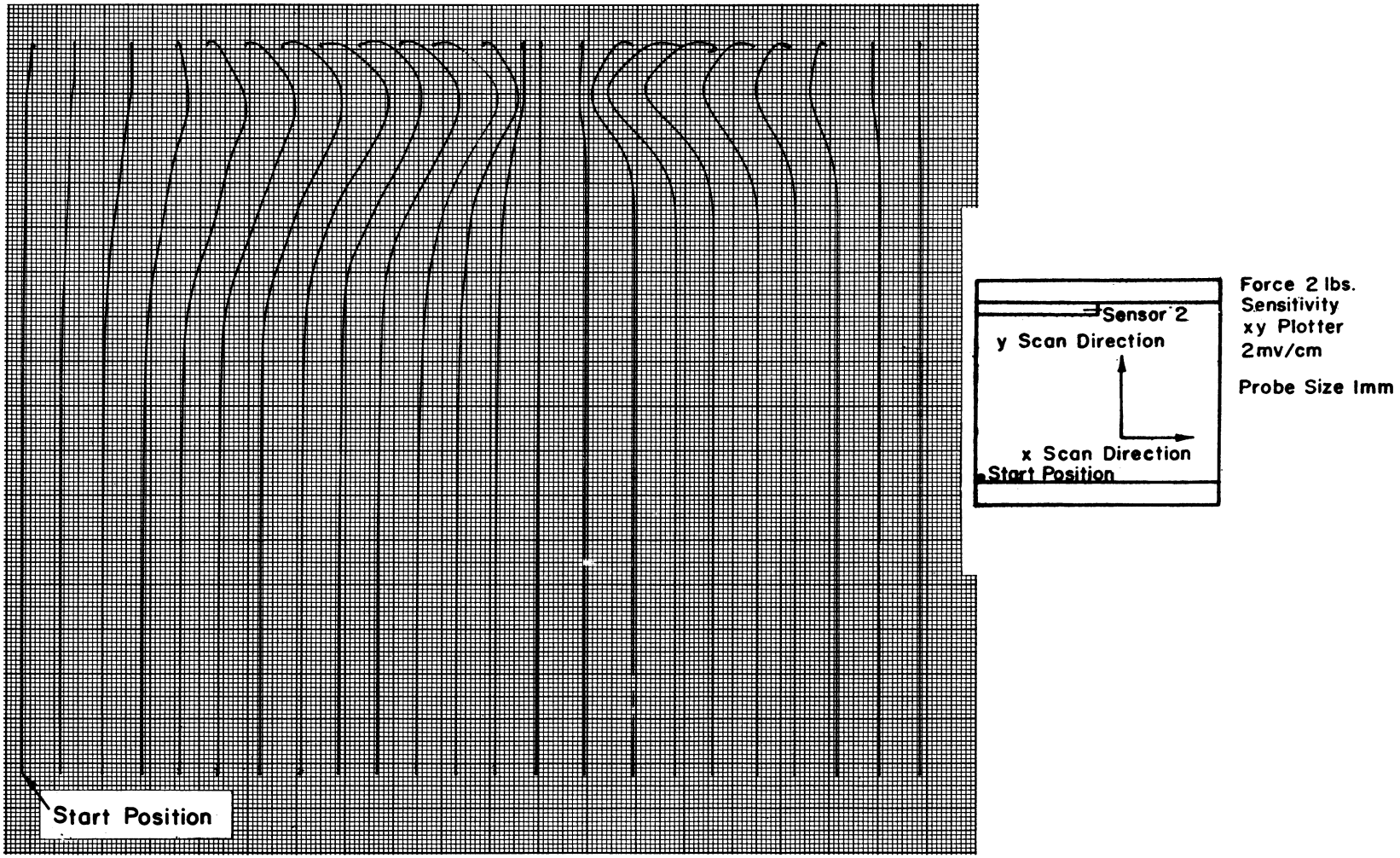

Figure 10. Flat occlusal surface.

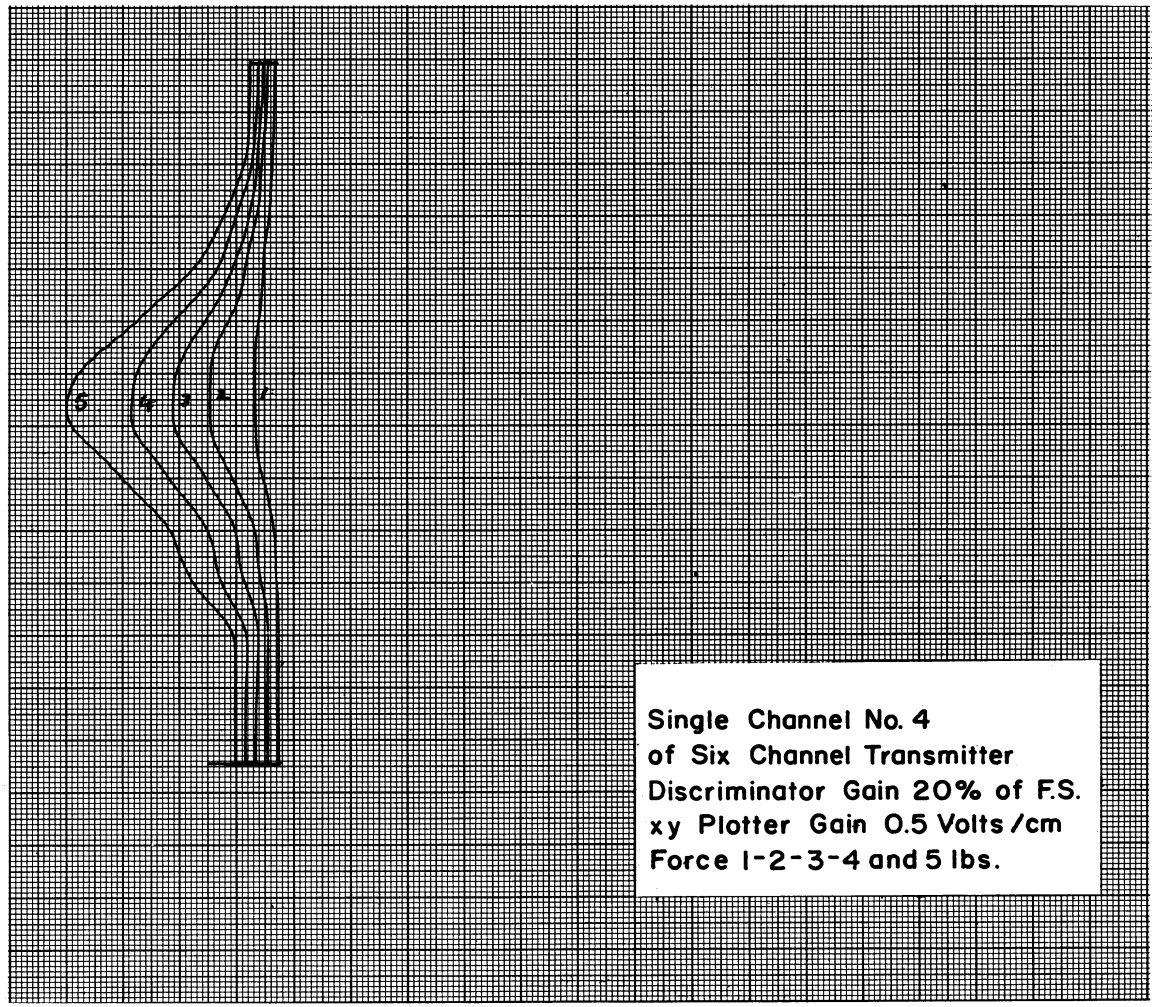

Figure 13. Force linearity test, normal occlusal surface.

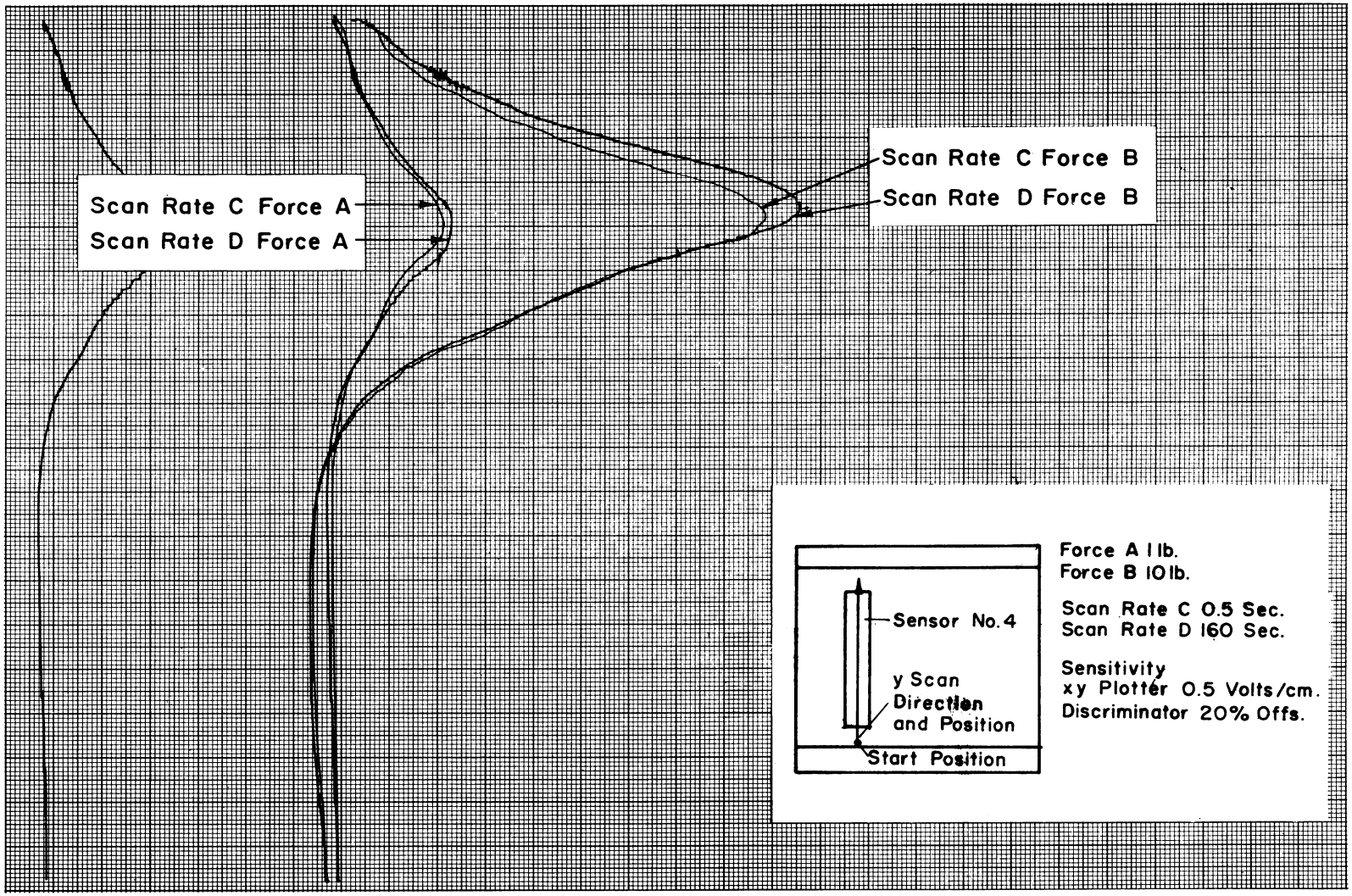

Figure 14. Scan rate response, normal occlusal surface.

D. COMPARISON BETWEEN THEORETICAL PREDICTIONS AND OBSERVED READINGS

The sensor calibration data presented in Figures 6-14 are quite similar in shape to those predicted analytically (see Figure 2). This indicates that the sensors are picking up only the tensile and compressive strain due to the point loadings and not the bearing strain also, as it might have been expected. Possibly, the force levels involved are low enough that the bearing stress does not significantly affect the sensor reading. Thus, the analysis which was based on the strain at a point within an infinite half-plane of material predicts the general shape of the curve obtained from the average strain over a volume in a relatively small amount of material. Near the sensor "edges" the agreement is poorest, as it would be expected.

The other significant agreement with the predictions is the linearity of the readings with the applied force. As shown in the previous section, the readings are linear enough that the calibration need only be done at a few force levels to adequately cover the entire range. This is valuable not only in the calibration, but also in the data analysis, since the simplest functional form between force points, a linear variation, may be used in the computer program.

ALTERNATE SENSOR CONFIGURATIONS

The present configuration of 6 sensors set in a "channel" provides an excellent basis for measurement of the 4 variables asscciated with a 2-component force acting on a (essentially) 2-dimensional surface. This particular idealization does not cover the possibility of multiple point contacts however. If multiple point contacts become of interest to the experimenter, 4 more sensors will be necessary for each additional contact point. Four are required, because each additional contact point has 2 dimensions and the force acting there also has 2 dimensions.

E. DATA ANALYSIS PROCEDURE

DATA ANALYSIS PROCEDURE

A flow chart showing the data analysis procedure is presented in Figure 15. The procedure is simply one of taking the digitized sensor output at discrete time intervals, comparing it to the calibration data to obtain the two-force and two-position components, then plotting these points in a suitable output format.

Calibration Data

The calibration data will be generated in essentially the same way that the data presented earlier in this report were taken. Namely, a known force will be applied at a known point on the occlusal surface and the resulting sensor outputs will be digitized and recorded on magnetic tape. Since the sensor output varies so nearly linearly with the force, it will only be necessary to use three-force points. Judging by the curves resulting from the present sensors, a spacing of about .010 in. (.25 mm) between contact point locations will be quite adequate to insure accuracy.

Raw Data

Once the system has been placed in the patient's mouth, the sensor outputs will be digitized and recorded on magnetic tape at discrete time intervals as the experiment proceeds.

Comparison of Raw Data to Calibration Data

The digitized raw data is then compared to the calibration data until the raw data point is bracketed by calibration data. Then, a linear interpolation between the calibration data points is made to predict the values of force and contact point location as accurately as possible.

So the procedure is (as shown in the flow chart, Figure 16) to store the calibration data, then, given a measurement S_1^*, S_2^*, S_3^*, S_4^*, search the S_1 data until S_1^* is bracketed by S_1^a and S_1^b, then test to determine if S_2^a and S_2^b bracket S_2^*. If not, continue the search on S_1 to find another set of values bracketing S_1^*. If yes, apply the test to $S_3^a < S_3^* < S_3^b$ or $< S_3^b < S_3^* < S_3^b$; then test S_4 similarly; if not, resume searching on S_1.

Now, once

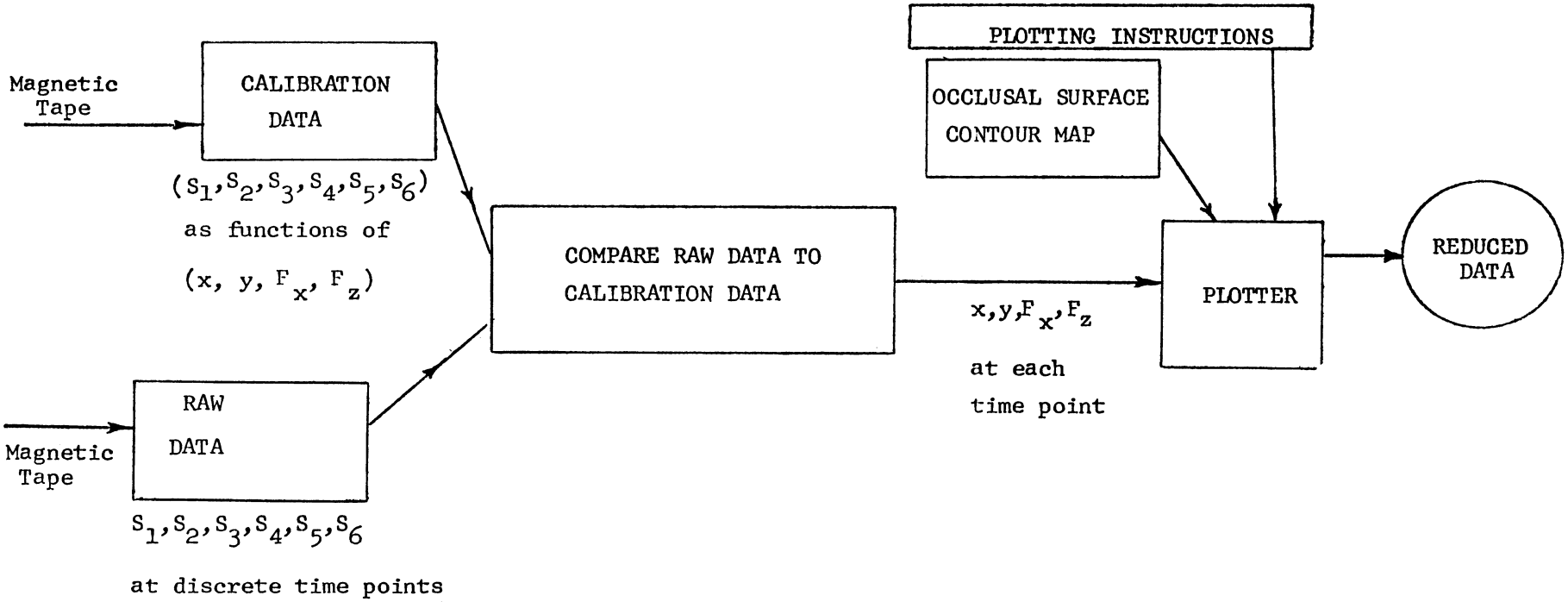

Figure 15. Data flow chart.

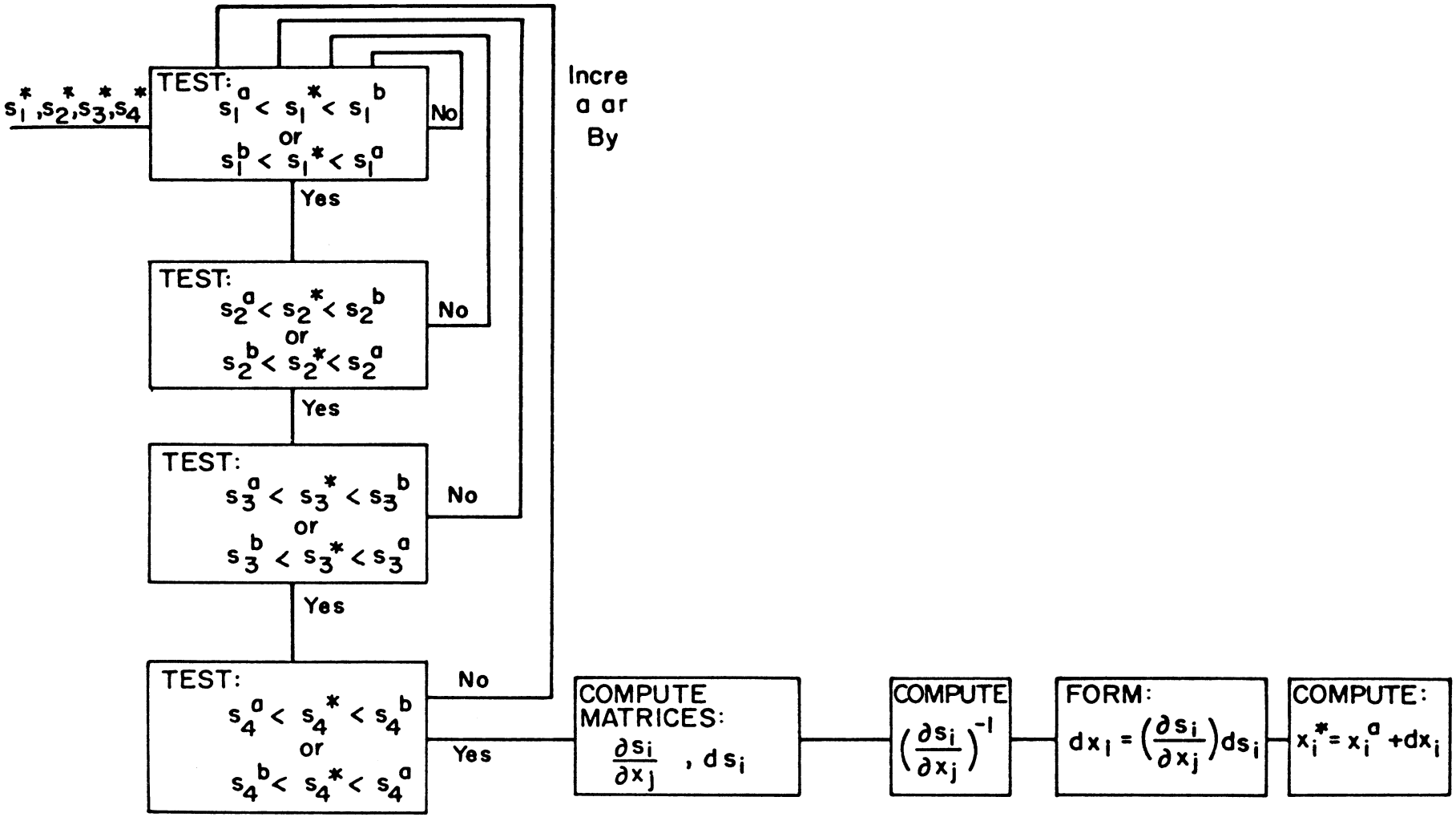

Figure 16. Data analysis flow chart.

$$S_1^a < S_1^* < S_1^b \qquad \text{or} \qquad S_1^b < S_1^* < S_1^a$$

and

$$S_2^a < S_2^* < S_2^b \qquad \text{or} \qquad S_2^b < S_2^* < S_2^a$$

and

$$S_3^a < S_3^* < S_3^b \qquad \text{or} \qquad S_3^b < S_3^* < S_3^a$$

and

$$S_4^a < S_4^* < S_4^b \qquad \text{or} \qquad S_4^b < S_4^* < S_4^a$$

Now, construct the matrix

$$\frac{\partial S_i}{\partial X_j} = \begin{pmatrix} \frac{S_1^a - S_1^b}{x^a - x^b} & \frac{S_1^a - S_1^b}{y^a - y^b} & \frac{S_1^a - S_1^b}{F_y^a - F_y^b} & \frac{S_1^a - S_1^b}{F_z^a - F_z^b} \\ \frac{S_2^a - S_2^b}{x^a - x^b} & \frac{S_2^a - S_2^b}{y^a - y^b} & \frac{S_2^a - S_2^b}{F_y^a - F_y^b} & \frac{S_2^a - S_2^b}{F_z^a - F_z^b} \\ \frac{S_3^a - S_3^b}{x^a - x^b} & \frac{S_3^a - S_3^b}{y^a - y^b} & \frac{S_3^a - S_3^b}{F_y^a - F_y^b} & \frac{S_3^a - S_3^b}{F_z^a - F_z^b} \\ \frac{S_4^a - S_4^b}{x^a - x^b} & \frac{S_4^a - S_4^b}{y^a - y^b} & \frac{S_4^a - S_4^b}{F_y^a - F_y^b} & \frac{S_4^a - S_4^b}{F_z^a - F_z^b} \end{pmatrix}$$

This matrix is used in the relationship between the differences between the observed signals and the ones from the calibration and the observed forces and contact points and the forces and contact points from the calibration.

The relationship is

$$dS_i = \frac{\partial S_i}{\partial X_j} \, dX_j$$

where

$$i = 1, 2, 3, 4 \quad \text{(sensor readings)}$$

$$X_j = (X, Y, F_y, F_z) \quad \text{(position and forces)}$$

Solving by inversion of the coefficient matrix,

$$\partial X_j = \left(\frac{\partial S_i}{\partial X_j} \right)^{-1} dS_i$$

Then, knowing the nearby calibration value and the differences in the forces and locations due to the difference between the observed value and the calibration, the final result may be expressed:

$$X^* = X_a + dx$$

$$Y^* = Y_a + dy$$

$$F_y^* = F_y^a + dF_y$$

$$F_z^* = F_z^a + dF_z$$

Plotter, Plotter Instructions, and Occlusal Surface Contour Map

The use of the plotter (on-line equipment at The University of Michigan's Computing Center) is recommended in order to be able to present the data to the experimenter in a form which is convenient for him to interpret.

One possible format is presented in Figure 17. This format requires that an occlusal surface map be made and digitized using the existing calibration equipment so that the plotter can accept it as input, redraw it, and plot the reduced data on it. The force data will be plotted alongside this position data. The number of points plotted on each diagram may be quite significant to the experimenter who is attempting to find patterns in the data. This number may be controlled by an arbitrary specification, or else fairly simple criteria may be adopted, e.g., the points may be plotted on a single diagram only when one of the force values crosses a preset threshold.

Another possible data format is shown in Figure 18. This format does not require the occlusal surface map, yet it might be used by the experimenter to find patterns in the force traces.

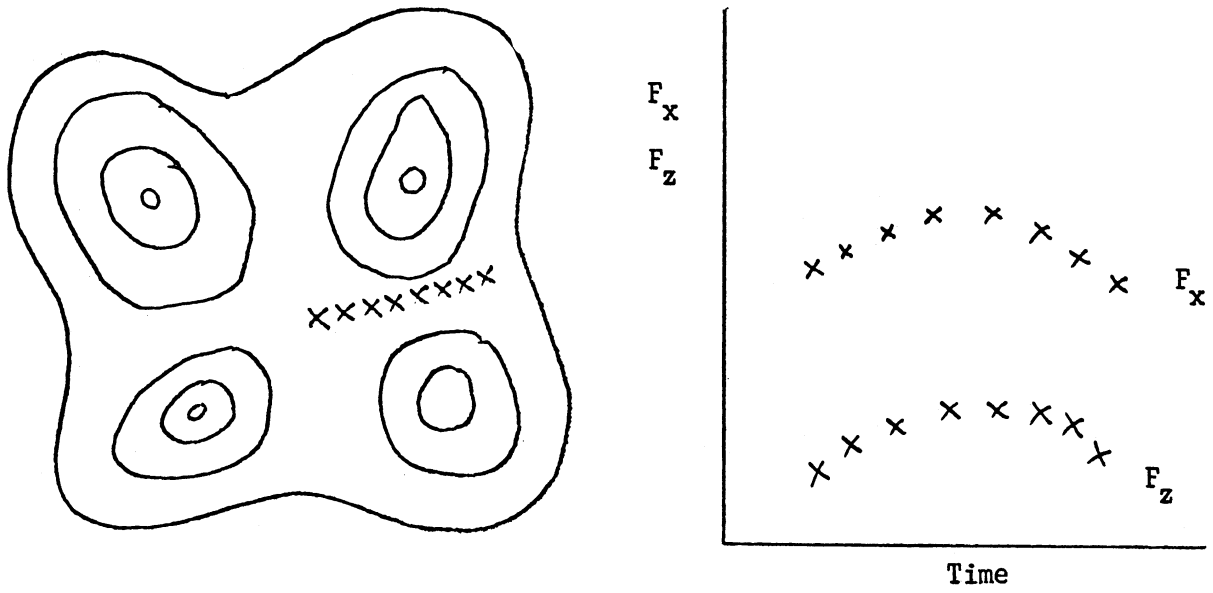

Figure 17. Suggested data output format.

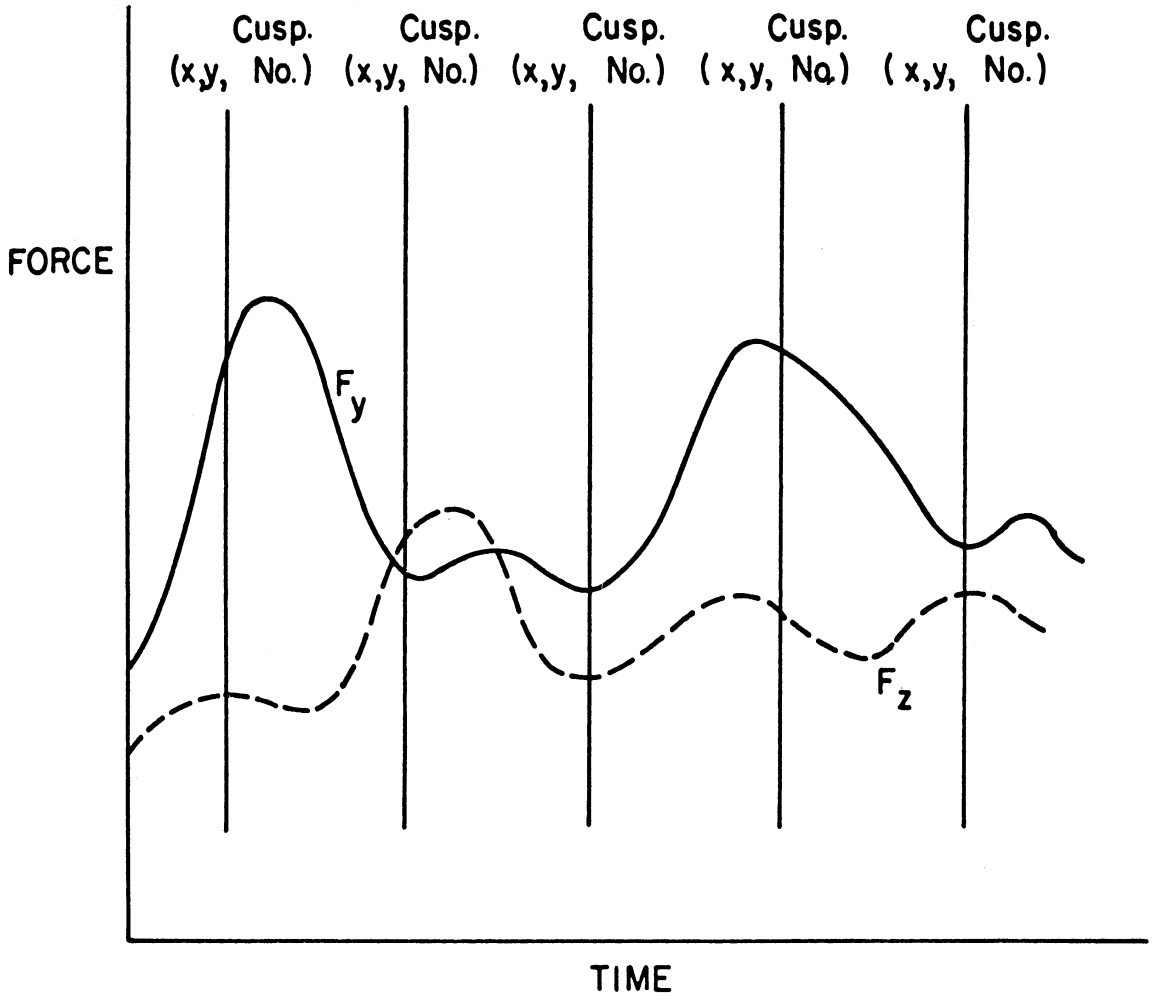

Figure 18. Possible data output format.

F. SUMMARY

The development of a device for calibrating six-channel intraoral transmitters has been accomplished and demonstrated to be necessary for obtaining reliable information on occlusal forces using solid state sensors and telemetry. It has also been shown that the interplay of complex occlusal forces requires sophisticated data analysis procedures and equipment.

In references to the objectives of the contract the following determinations have been made and are included in this report:

1. A theoretical analysis of the problems associated with calibration of the transmitters showed that the output of a sensor could follow that shown in Figure 2. The data derived during calibration procedures (Figures 6-14) indicate that the response of the sensors in an acrylic medium was quite similar to the predicted response.

2. The theoretical analysis indicating the use of six sensors was also borne out by laboratory tests with the calibration device. This geometrical configuration has been shown in Figure 5.

3. The calibration system which was designed and fabricated has been shown to provide accurate and reproducable loading of occlusal surfaces. Both velocity of traverse loading and variation in loading is possible with the device. In addition, the form, size, contact points, and types of contact can be altered to determine sensor responses under varying conditions.

4. The output of the sensors was found to be linear relative to speed of traverse loading and variations in loading. Repeated scanning of the sensors in identical planes indicates that the sensors are responding to the same loads in an identical manner.

5. The data analysis procedure which has been described is compatible with existing techniques of data analysis and reduction.